The Astronomical Journal, 128:2265–2273, 2004 November

THE METALLICITY DISTRIBUTION OF F/G DWARFS DERIVED FROM BATC SURVEY DATA

Cui-hua Du,[1,2] Xu Zhou,[1] Jun Ma,[1] Jian-rong Shi,[1] Alfred Bing-Chih Chen,[3]
Zhao-ji Jiang,[1] and Jian-sheng Chen[1]
Received 2004 May 13; accepted 2004 July 29

ABSTRACT

Based on synthetic flux spectra calculated from theoretical atmospheric models, a calibration of temperature and metallicity for the dwarfs observed in the Beijing-Arizona-Taiwan-Connecticut multicolor photometric system is presented in this paper. According to this calibration, stellar effective temperatures can be obtained from some temperature-sensitive color indexes. The sample stars have colors and magnitudes in the ranges $0.1 < d - i < 0.9$ and $14.0 < i < 20.5$. The photometric metallicities for these sample stars can be derived by fitting SEDs. We determine the average stellar metallicity as a function of distance from the Galactic plane. The metallicity gradient is found to be $d[\mathrm{Fe/H}]/dz = -0.37 \pm 0.1$ dex kpc^{-1} for $z < 4$ kpc and $d[\mathrm{Fe/H}]/dz = -0.06 \pm 0.09$ dex kpc^{-1} between 5 and 15 kpc. These results can be explained in terms of different contributions in density distribution for Galactic model "thin disk," "thick disk," and "halo" components. However, for the gradient in $z > 5$ kpc, it could not be interpreted according to the different contributions from the three components because of the large uncertainty. So it is possible that there is little or no gradient for $z > 5$ kpc. The overall distribution shows a metallicity gradient $d[\mathrm{Fe/H}]/dz = -0.17 \pm 0.04$ dex kpc^{-1} for $z < 15$ kpc.

Key words: Galaxy: abundances — Galaxy: disk — Galaxy: formation — Galaxy: halo — Galaxy: structure

1. INTRODUCTION

The Galaxy is unique in offering the possibility of determining directly the three-dimensional distributions of luminous mass and chemical abundances. The combination of these results allows us to conduct a detailed investigation of the dominant physical processes that occurred during the formation and early evolution of the Galaxy (Gilmore & Wyse 1985). Over the past decade considerable effort has been devoted to gaining information about the structure and formation of the Galaxy.

Of crucial importance in the structure and formation of the Galaxy is the existence of a thick-disk component. Ever since it was revealed that the Galactic disk contains two distinct stellar populations, the origin and nature of the difference have been discussed by a number of investigators. The thick-disk population was evident in the data of Hartkopf & Yoss (1982) and clearly explained by Gilmore & Reid (1983). While subsequent investigations have determined the overall kinematic and chemical properties of the thick disk rather well (Gilmore & Wyse 1985; Sandage & Fouts 1987; Majewski 1992; Reid & Majewski 1993; Robin et al. 1996), the relation of the thick disk to the halo population and to the thin disk, as well as its evolutionary history, are still poorly known (Gilmore et al. 1989). In addition, the formation of the thick-disk component remains an open question. A number of models for the formation of the thick disk have been put forward since the confirmation of its existence. Sandage (1990) proposed that the thick disk was formed by dissipative pressure-supported collapse in the early history of the Galaxy, producing a kinematic and chemical gradient as the gas was settling into the Galactic plane. Other scenarios of the thick-disk formation, including one in which the thick disk is the result of an accretion-induced heating of the thin disk, were discussed by Majewski (1993). To study the formation process of the thick disk in more detail, additional information such as the metallicity gradient is also needed. If this detailed information becomes available, it might provide clues concerning not only the formation history of the thick disk but also of the Galaxy as a whole.

Numerous surveys along the Galactic plane have been used to investigate the existence and size of the Galactic radial abundance gradient in the disk. A wide variety of objects have been used to determine this gradient, including radio and optical observations of H II regions, disk stars (Neese & Yoss 1988), planetary nebulae (Shaver et al. 1983; Pasquali & Perinotto 1993; Henry & Worthey 1999; Hou et al. 2000; Maciel et al. 2003), and open clusters (Friel 1995; Chen et al. 2003). The existence of a radial gradient in the Galaxy is now well established. An average gradient of about -0.06 dex kpc^{-1} is observed in the Galactic disk for most of the elements (Chen et al. 2003). On the other hand, considerable disagreement exists about whether there is a vertical metallicity gradient among the field and/or open-cluster stars of the Galactic disk. What its extent would be and the reasons for it are not well understood either; yet potentially it could provide a powerful clue concerning Galactic formation. The amplitude of any vertical gradient of stellar properties allows us to place constraints on the existence of a discrete stellar subpopulation and/or distinct components of the Galaxy (Sandage 1981).

The Beijing-Arizona-Taiwan-Connecticut (BATC) multicolor photometric survey accumulated a large database that is very useful for studying the structure and formation of the main components of the Galaxy. Du et al. (2003) provided information on the density distribution of the main components of the Galaxy that can be used to impose constraints on the parameters of models of the Galactic structure. Here, we use F and G dwarfs from the BATC survey data to provide the metal abundance information. The main-sequence lifetime of F- and G-type stars is longer than the age of the Galaxy, and hence the chemical

[1] National Astronomical Observatories, Chinese Academy of Sciences, Beijing 100012, China; dch@vega.bac.pku.edu.cn.
[2] College of Physical Sciences, Graduate School of the Chinese Academy of Sciences, Beijing 100012, China.
[3] Department of Physics, National Cheng Kung University, Taiwan 70148, Taiwan.

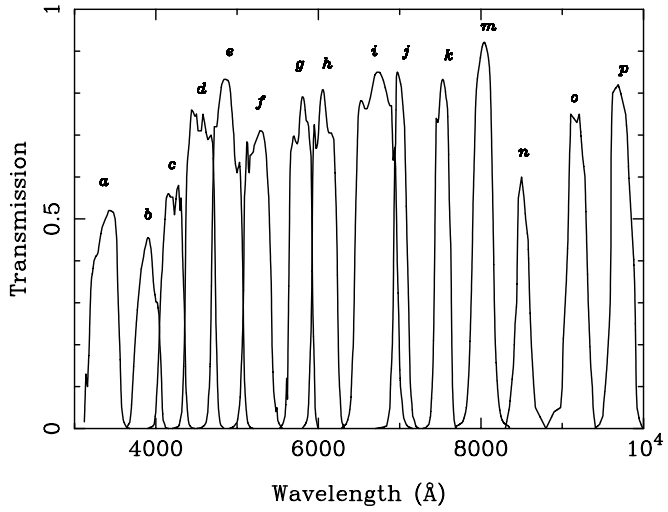

FIG. 1.—Transmission curves for the BATC multicolor filters.

abundance distribution function of such stars provides an integrated record of the chemical enrichment history (Chen et al. 2000b). Many general trends have been discovered during the past decades. With recent improvements in observations and improved knowledge regarding galaxy formation, it becomes possible to further discuss the metallicity gradient in the Galaxy.

In this paper, we attempt to study the metallicity gradient of the Milky Way galaxy using the BATC photometric survey data. The outlines of this paper is as follows. The BATC photometric system and data reduction are introduced briefly in § 2. In § 3 we describe the theoretical model atmosphere spectra and synthetic photometry. In § 4 we present the BATC data used in this analysis. The vertical metallicity gradient is discussed in § 5. In § 6 an estimation for metallicity gradient using a three-component model is made, and the result is compared with the observed metallicity gradient. Finally, in § 7 we summarize our main conclusions in this study.

2. BATC PHOTOMETRIC SYSTEM AND DATA REDUCTION

The BATC program uses the 60/90 cm f/3 Schmidt telescope at the Xinglong Station of the National Astronomical Observatories (NAOC), with a 2048×2048 Ford CCD mounted at its focal plane. The field of view of the CCD is $58' \times 58'$, with a pixel scale of $1''.7$. There are 15 intermediate-band filters in the BATC filter system, which covers an optical wavelength range from 3000 to 10000 Å. Figure 1 shows the filters transmissions. The well-known advantage of using these filters is that in intermediate bandwidths it is possible to ignore the color terms for atmospheric-extinction correction, whereas they must be taken into account with broadband filters. The BATC magnitudes use the monochromatic AB magnitudes as defined by Oke & Gunn (1983). The standard stars HD 19445, HD 84937, BD $+26^{\circ}2606$, and BD $+17^{\circ}4708$ (Oke & Gunn 1983) are observed for flux calibration in the BATC survey. A detailed description of the BATC photometric system and flux calibration of the standard stars can be found in Fan et al. (1996) and Zhou et al. (2001, 2003).

The BATC survey images were reduced using standard procedures, including bias subtraction, flat-field correction, and flux calibrations (Fan et al. 1996; Zhou et al. 2001, 2003). After the basic corrections described above, the multiple field images observed of each filter were combined by integer pixel shifting for each one. The cosmic rays and bad pixels were corrected for when the images were combined through a comparison of multiple images. The *HST* Guide Star Catalog (GSC) (Jenkner et al. 1990) was then used for coordinate determination. The final rms error in the positions of GSC stars is about $0''.5$. The magnitudes of the point sources in the BATC fields are measured using the photometric method of point-spread function (PSF) fitting. Our PSF magnitudes were obtained through an automatic data reduction program PIPELINE 2, which was developed based on Stetson's DAOPHOT procedures (Stetson 1987). Finally, at the completion of photometry the spectral energy distribution (SEDs) of all measurable objects are obtained.

3. THEORETICAL MODEL AND CALIBRATION FOR TEMPERATURE AND METALLICITY

3.1. *Theoretical Stellar Library and Synthetic Photometry*

A homogeneous and complete stellar library can meet the most ambitious goals intended for a standard library. Lejeune et al. (1997) presented a hybrid library of synthetic stellar spectra. The library covers a wide range of stellar parameters: $T_{\rm eff} = 50{,}000$–2000 K in intervals of 250 K, $\log g = -1.02$–5.50 in main increments of 0.5, and $[{\rm M/H}] = -5.0$–1.0. For each model in the library, a flux spectrum is given for the same set of 1221 wavelength points covering the range 9.1–160,000 nm, with a mean resolution of 20 Å in the visible. The spectra are thus in a format that has proved to be adequate for synthetic photometry of wide- and intermediate-band systems.

On the basis of the theoretical library, we calculate the synthetic colors of the BATC system. Here, we synthesize colors for simulated stellar spectra with $T_{\rm eff}$ and $\log g$ characteristic of F/G dwarfs ($\log g = 4.0,\ 4.5$ for dwarfs) and 19 values of metallicity ($[{\rm M/H}] = -5.0, -4.5, -4.0, -3.5, -3.0, -2.5, -2.0, -1.5, -1.0, -0.5, -0.3, -0.2, -0.1, 0.0, +0.1, +0.2, +0.3, +0.5$, and $+1.0$), where [M/H] denotes metallicity relative to hydrogen. The synthetic ith BATC filter magnitude can be calculated with

$$m = -2.5\log\frac{\int F_\lambda \phi_i(\lambda) d\lambda}{\int \phi_i(\lambda) d\lambda} - 48.60, \qquad (1)$$

where F_λ is the flux per unit wavelength, ϕ_i is the transmission curve of the ith filter of the BATC filter system (Fig. 1). In Figure 2, as an example, we present the two-color diagram based on the c, i, and p filters. From this figure, we can clearly see how the color indexes vary as a function of temperature and metallicity. In this two-color diagram, the gravity $\log g = 4.5$ corresponds roughly to dwarfs. Four metallicities ($[{\rm M/H}] = -5.0, -1.5, 0.0$, and $+1.0$) are arbitrarily selected and the temperature range is $5000\ {\rm K} \le T_{\rm eff} \le 8000$ K. For clarity, the grid points are connected with lines, illustrating the isothermal and isometallicity lines. Similar grids, of course, exist as well for other two-color diagrams with different gravities and metallicities in the library.

The bluer colors are sensitive to metallicity down to the lowest observed metallicities because most of the line-blanketing from heavy elements occurs in the shorter wavelength regions. In contrast, the redder colors are primarily sensitive to the temperature index. The BATC a and b bands contain the Balmer jump, a stellar spectral feature that is sensitive to surface gravity. Since our sample includes only F/G dwarfs, it conveys little gravity information. Therefore, in the following sections,

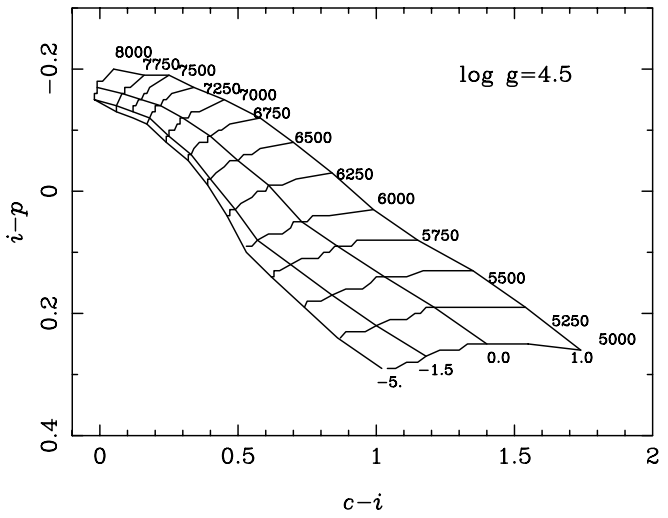

FIG. 2.—The $i - p$ vs. $c - i$ diagram. A grid of constant-log g models with the metallicities: [M/H] = −5.0, −1.5, 0.0, and +1.0; and with $T_{\rm eff} \geq 5000$ K are presented in the two-color diagram. The grid points are connected with straight lines, illustrating isotherm and isometallicity lines.

we focus on effective temperature and metallicity. It should be mentioned that, although the metallicity or temperature derived from synthetic photometry is not very accurate for a single star, which might be distorted by a poor point, they can be made meaningful by studying a sample of stars.

3.2. *Temperature and Color Index*

The stellar effective temperature can be derived by comparing observed SEDs with theoretical ones. In general, a sensitive color index can represent this physical quantity, such as $b - y$ in the *ubvy* system (Ardeberg et al. 1983). We would like to find such color indexes that are sensitive to the effective temperature in the BATC filter system. Our study shows that color indexes $d - n$, $d - o$, $e - o$, and $e - p$ are very sensitive to temperature but are relatively insensitive to log g and [M/H]. In Figure 3, the relationships between log $T_{\rm eff}$ and color index are shown, and the correlation between log $T_{\rm eff}$ and color index is nearly linear. The dots represent a grid of theoretical models for different-metallicity F/G dwarfs. As shown in Figure 3, a simple polynomial can describe the relationship between log $T_{\rm eff}$ and the color indexes. A quadratic polynomial is as follows:

$$\log T_{\rm eff} = A_0 + A_1({\rm CI}) + A_2({\rm CI})^2, \qquad (2)$$

where CI is the color index. The coefficients of equation (2) for different color indexes are listed in Table 1. The final photometric effective temperature can be derived by taking the mean value among the four temperatures from the different color indexes. Chen et al. (2000a) used the most temperature-sensitive color index in their study to derive the effective temperature. Our results show that our fitting on $d - o$ is very close to the red region of their fitting on NGC 288 stars.

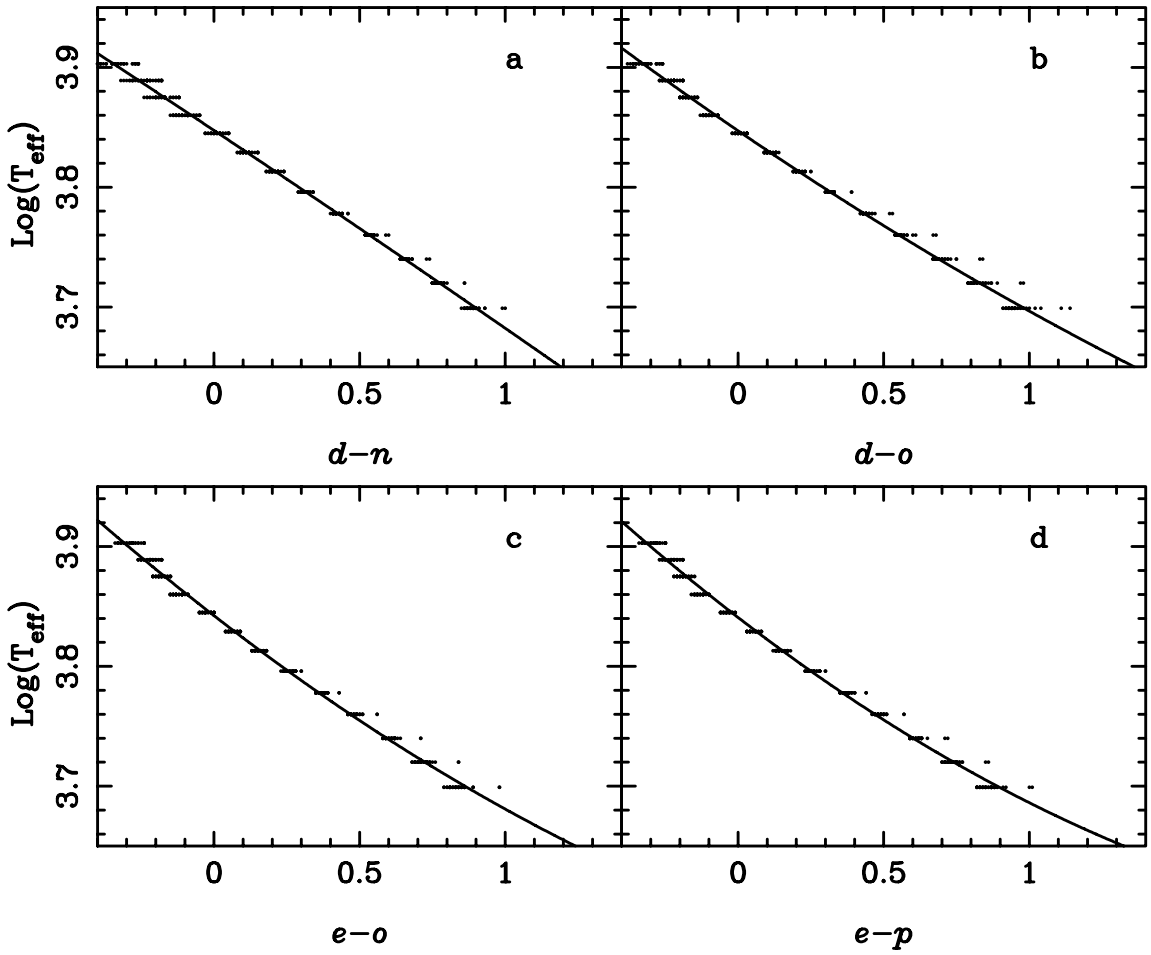

FIG. 3.—Relationship between log $T_{\rm eff}$ and the color indexes of bandpasses relatively insensitive to log g in our data for (*a*) $d - n$, (*b*) $d - o$, (*c*) $e - o$, and (*d*) $e - p$. The symbol dots represent a grid of theoretical models for different-metallicity dwarfs.

TABLE 1
Coefficients of the Color Index and Effective Temperature Relation

Color Index	A_0	A_1	A_2	χ^2
$d-n$	3.8474	−0.1620	−0.0031	0.011
$d-o$	3.8471	−0.1663	0.0158	0.011
$e-o$	3.8423	−0.1884	0.0270	0.013
$e-p$	3.8408	−0.1873	0.0327	0.013

3.3. *Metallicity and Abundance*

Photometric indices have often been used to give the stellar metallicity. For example, Wallerstein (1962) derived the [Fe/H] calibration using the $\delta(U-B)$ excess of the Johnson *UBV* photometric system. For the *uvby* system, Crawford (1975a), Nissen (1981), and Olsen (1988) used the photometric differentials δm_1 and δc_1 to derive the [Fe/H] calibration. Following that, Schuster & Nissen (1989) made direct use of the photometric indices m_1 and c_1 to derive [Fe/H] calibrations for F and G dwarfs.

For the BATC multicolor photometric system, there are 15 intermediate-band filters covering an optical wavelength range from 3000 to 10000 Å. So the SEDs of 15 filters for every observed object are equivalent to a low-resolution spectrum. Using equation (2), we can derive the effective temperature of a given star in advance from the available photometry. Thus, given a photometrically determined effective temperature, we can use the SED simulation to derive the stellar metallicity. The standard χ^2 minimization, i.e., computing and minimizing the deviations between the photometric SED of a star and the template SEDs obtained with the same photometric system, is used in the fitting process. The minimum $\chi^2_{\rm min}$ indicates the best fit to the observed SED by the set of template spectra:

$$\chi^2 = \sum_{l=1}^{N_{\rm filt}=15} \left(\frac{m_{{\rm obs},l} - m_{{\rm temp},l} - b}{\sigma_l} \right)^2, \qquad (3)$$

where $m_{{\rm obs},l}$, $m_{{\rm temp},l}$, and σ_l are the observed magnitude, template magnitude, and their uncertainty in filter l, respectively, and $N_{\rm filt}$ is the total number of filters in the photometry, while b is the mean magnitude difference between observed magnitude and template magnitude. The uncertainties of metallicity obtained from a comparison between SED photometry and theoretical models are due to the observational error and the finite grid of the models (Chen et al. 2000a). For the metal-poor stars ([Fe/H] < -1.0), the metallicity uncertainty is about 0.5 dex and 0.2 dex for the stars with [Fe/H] > -0.5.

4. PHOTOMETRIC DATA

4.1. *Object Classification and Photometric Parallaxes*

In this study, we use the following two fields at intermediate latitudes:

1. The BATC T329 field, with central coordinates $\alpha = 09^{\rm h}53^{\rm m}13^{\rm s}.30$ and $\delta = 47^\circ49'00''.0$ (J2000) (Galactic coordinates: $l = 169^\circ.95$, $b = 49^\circ.80$). It is complete to 20.5 mag, with an error of less than 0.1 mag in the BATC *i* band. Each object is classified according to its SED information constructed from the 15-color photometric catalog. The observed colors of each object are compared with a color library of known objects with the same photometric system. First, we use spectral templates of galaxies and stars to discriminate the stars from galaxies. The profile of objects classified as stars does not deviate significantly from that of stellar templates. The input library for stellar spectra is the Pickles (1998) catalog. Details about the classification of the galaxies are given in Xia et al. (2002) and details about the classification of stars in Du et al. (2003). The limiting magnitude is not so deep as to be strongly contaminated by a lot of galaxies, with the possibility of galaxy contamination estimated to be less than 3%.

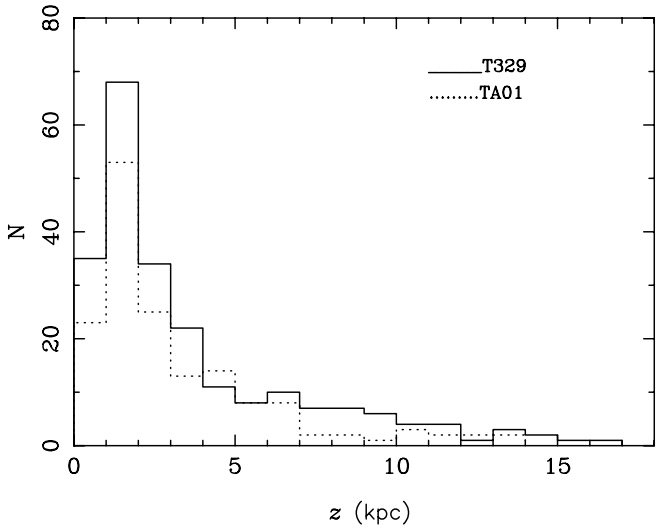

Fig. 4.—Distribution of z distance in the two fields. The solid line represents the T329 field, and the dotted line represents the TA01 field.

2. The BATC TA01 field with central coordinates $\alpha = 01^{\rm h}12^{\rm m}06^{\rm s}.00$ and $\delta = -00^\circ02'00''$ (J2000) (Galactic coordinates: $l = 134^\circ.16$, $b = -62^\circ.45$). It is complete to 20.0 mag in the BATC *i* band. It should be noted that the stars-galaxies separation for the BATC TA01 field is different from the BATC T329 field. Because the BATC TA01 field has been observed by the Sloan Digital Sky Survey (SDSS) and each object type (stars-galaxies-QSO) has been given, we can make direct use of those stars to obtain star types according to the stellar spectra library.

According to the results of object classification, we pick out the F/G dwarfs from the two fields. In total, there are 383 F/G dwarfs, and the photometric parallaxes can be obtained according to the stellar types. In Figure 4, we give the actual z distance distribution for two fields. It is clear that most of stars are in the range $z \sim 1$–2 kpc for the two fields. A variety of errors affect the determination of stellar distances. The first source of errors is from a photometric uncertainty of less than 0.1 mag in the BATC *i* band; the second from the misclassification, which should be small because of the multicolor photometry. For luminosity class V, types F/G, the absolute magnitude uncertainty is about 0.3 mag. In addition, there may exist an error from the contamination of binary stars in our sample. We neglect the effect of binary contamination on distance derivation due to the unknown but small influence from mass distribution in binary components (Kroupa et al. 1993; Ojha et al. 1996). The two fields lie in intermediate latitudes and the influence of interstellar extinction in the distance calculation can be neglected.

4.2. *Classification Comparison and Stellar Population*

A comparison of the stellar classifications is made between those in the stellar spectra library of Pickles (1998) and the theoretical spectra library of Lejeune et al. (1997). In our previous paper (Du et al. 2003), we derived the stellar type

TABLE 2

Classification Comparisons between Stellar Synthetic Spectra from Lejeune et al. (1997) and Stellar Library from Pickles (1998)

Type	$T_{\rm eff}$	[Fe/H]	log g	V	r (kpc)
G8 V	5110	−2.0	4.5	18.2	2.9
G5 V	5330	−1.0	4.5	17.2	2.4
G3 V	5470	−0.5	4.0	16.1	1.8
G0 V	5717	−1.0	4.5	16.5	2.4
F7 V	6047	−0.3	4.5	14.6	1.5
F5 V	6273	−3.5	4.0	17.0	4.0

according to the Pickles stellar spectra library (Pickles 1998). To obtain more information about metallicity, here we use the theoretical spectra library from Lejeune et al. (1997) to derive the stellar parameters such as temperature and metallicity. To check the agreement between the Pickles and Lejeune libraries, we present a comparison.

As an example, Table 2 lists the comparison results between the Pickles and Lejeune spectra for six stars in our sample. The first column is the stellar type derived from Pickles library. According to the theoretical library of Lejeune et al. (1997), the effective temperature $T_{\rm eff}$ is determined using equation (2), and it is listed in the second column. The gravity log g and metallicities [Fe/H] are also derived by fitting SEDs according to the theoretical library of Lejeune et al. (1997). They are listed in the following two columns. The apparent visual magnitude V and photometric distances are listed in the last two columns. As listed in Table 2, our classification results from the Pickles library are in excellent agreement with the theoretical library of Lejeune et al. (1997). The metallicities [Fe/H] for these stars can only provide an estimate of individual stellar abundances, but we have the advantage of being able to use many stars to obtain mean metallicity at different distances from the plane.

Standard star-count models indicate that the color-magnitude range could be used to separate roughly different populations of the Galaxy (Chen et al. 2001; Du et al. 2003). The present sample stars have colors and magnitudes in the ranges $0.1 < d - i < 0.9$ and $14.0 < i < 20.5$. According to star-count models, the present sample should contain predominantly thick-disk stars in this color-magnitude range, with some contributions from the thin disk and halo near the edge of the sample selection. As shown in Figure 5, there are no stars redder than $d - i \sim 0.9$. For the T329 field, the star distribution is smooth, while there is a sharp increase at $d - i \sim 0.6$ for the TA01 field. The peak values for the two fields, however, lie in $d - i \sim 0.6$. We use the Galaxy models to predict the relative frequency of dwarfs belonging to each of the three dominant components in the Galaxy. These relative frequencies obviously depend on both the local normalization of each component's density distribution and its scale height. The density distributions can be combined with the local volume element to produce estimates of the number of stars from given components expected to be observed at a given height above the plane (Gilmore & Wyse 1985),

$$n_i(z) = \rho_{0i} \exp(-z/z_{0i}) z^2 dz, \quad (4)$$

where the subscript i refers to each component, ρ_0 is the local density normalization, and z_0 is the scale height. The components are (1) the thin disk with local normalization 1.0 and an exponential scale height of 320 pc (Du et al. 2003); (2) the thick disk, with local normalization 0.07 and exponential scale height of 640 pc (Du et al. 2003); and (3) the halo, with local a normalization of 0.00125 and an $R^{1/4}$ density distribution with axial ratio of 0.6 and an effective radius of 2.7 kpc (Du et al. 2003). The resulting curves for various components of the Galaxy are shown in Figure 6. The solid line, dotted-dashed line, and dotted line represent the contribution of the halo, thick disk, and thin disk, respectively. The various curves are normalized independently of each other. In Table 3, we show the logarithmic numbers as functions of height. The number of stars in the thin disk, thick disk, and halo are represented by n_0, n_1, and n_2, respectively. The curves in Figure 6, when combined with local normalization, mean that the thin disk will contribute up to z heights of about 1 kpc, while the thick disk will dominate from 1 to 4 kpc.

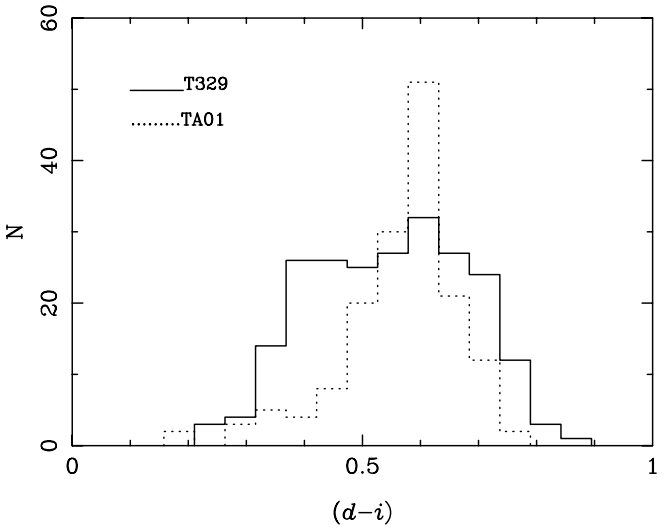

Fig. 5.—Distribution of $d - i$ in the two fields. Lines are as in Fig. 4.

5. THE VERTICAL METALLICITY GRADIENT TOWARD HIGH-LATITUDE FIELDS

It is well known that the chemical abundance of a stellar population contains much information about the population's early evolution, whereas detailed information about the vertical

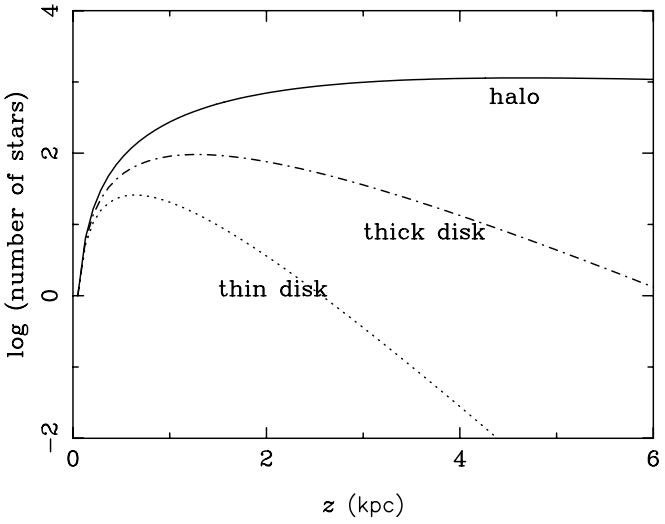

Fig. 6.—Relative number of stars within a given volume element as a function of height above the plane for various components of the Galaxy.

TABLE 3
THE NUMBER OF STARS VERSUS THE DISTANCE z FOR THREE COMPONENTS OF THE GALAXY

z (kpc)	log n_0	log n_1	log n_2
0.05	4.03	2.91	1.19
0.69	5.44	4.76	3.36
1.34	5.13	4.89	3.81
1.98	4.60	4.79	4.03
2.63	3.97	4.60	4.14
3.27	3.28	4.35	4.20
3.92	2.57	4.07	4.23
4.57	1.82	3.77	4.24
5.21	1.06	3.44	4.24
5.86	0.29	3.11	4.23

metallicity gradient can provide an important clue about the formation scenario of stellar populations. The metallicity distribution of stars in the Galaxy has been the subject of several spectroscopic and photometric surveys (Yoss & Hartkopf 1979; Hartkopf & Yoss 1982; Gilmore & Wyse 1985; Ratnatunga & Freeman 1989; Friel 1988).

The existence of a vertical metallicity gradient among field and open cluster stars of the Galactic disk is controversial. For example, using DDO photometry of the late-type giants in the direction of both Galactic poles, several authors found a vertical gradient ranging from approximately -0.2 to -0.4 dex kpc^{-1} (see Hartkopf & Yoss 1982; Yoss et al. 1987; Norris & Green 1989). Other independent studies have also shown evidence for a significant vertical gradient: Buser & Rong (1995), using the photographic *RGU* data to study the metallicity distribution of the Galactic components, found a vertical abundance gradient of -0.6 dex kpc^{-1} for the old thin disk and a marginal metallicity gradient of -0.1 dex kpc^{-1} for the thick disk. Robin et al. (1996) showed that the data toward the pole are in favor of a small gradient of -0.25 dex kpc^{-1}, data in SA54 field (Yamagata & Yoshii 1992) give a high value of -0.65, while data from Fenkart & Esin-Yilmaz (1985) favor a small gradient of -0.15 dex kpc^{-1}. However, Gilmore & Wyse (1985) showed that there is little or no gradient in the three components of the Galaxy.

Recent work has used open clusters instead of field stars to determine the metallicity gradient perpendicular to the disk. Piatti et al. (1995) found a correlation between [Fe/H] and vertical position, and they obtained a gradient equal to -0.34 dex kpc^{-1} by binning the data in z. Carraro et al. (1998) also derived a vertical abundance gradient of -0.25 dex kpc^{-1}. Cameron (1985) used metallicities determined from *UBV* photometry and found no gradient perpendicular to the plane. Friel (1995) did not find a gradient from the study of open clusters either.

In this study, we want to show how the BATC survey data can limit possible metallicity gradients for the components of the Galaxy. At first, the metallicity for the sample F/G dwarfs can be derived by comparing SEDs between photometry and theoretical models. The SEDs fitting method is described in § 3.3. In Figures 7*a*–7*e*, the metallicity distributions are shown as functions of apparent magnitude for sample stars. Figure 7*f* gives the metallicity distribution for all stars. Here, we divide these F/G dwarfs into five bins: $14.0 < i \leq 15.5$, $15.5 < i \leq 16.5$, $16.5 < i \leq 17.5$, $17.5 < i \leq 18.5$, and $i > 18.5$ to see how the magnitude affects the abundance distribution. From the figures (Figs. 7*a*–7*e*), we can see that there is a shift from metal-rich stars to metal-poor ones with the increase of apparent magnitude. The shift is particularly apparent in Figure 8, where the mean metallicity as a function of z-distance is displayed for the combined sample. It should be noted that we use the mean metallicity to describe the metallicity distribution function. We adopt the "biweight" statistical method provided by ROSTAT software (Beers et al. 1990) to estimate the stellar mean metallicity. Although computationally more complex, the biweight estimate has proved to be superior in many respects and has also performed well for small samples. Karaali et al. (2003) showed that the mean value is also valid to describe a distribution function.

As Figure 8 shows clearly, the mean metal abundance decreases with the increasing mean z, indicating a clear vertical metallicity gradient of the disk ($z < 4$ kpc). The individual fields give essentially the same result and have therefore been combined to improve the statistics. The T329 field lies in northern latitude direction and TA01 field in southern latitude direction. In addition, the distributions in the two fields do not differ significantly in number of stars, so we can combine them. The overall distribution shows a metallicity gradient $d[\mathrm{Fe/H}]/dz = -0.17 \pm 0.04$ dex kpc^{-1}, up to 15 kpc. At the same time, we find a gradient of -0.37 ± 0.1 dex kpc^{-1} for $z < 4$ kpc, whereas it shows a weak or zero gradient between 5 and 15 kpc, i.e., $d[\mathrm{Fe/H}]/dz = -0.06 \pm 0.09$ dex kpc^{-1}.

Based on Geneva photometry, Grenon (1977) investigated the vertical metallicity gradient for G and K giants and estimated a value of -0.35 dex kpc^{-1} for z between 0 and 700 pc. Yoss et al. (1987) obtained G5–K6 giants near the Galactic poles and found a chemical gradient of -0.4 dex kpc^{-1} for the thin disk and a gradient of -0.18 dex kpc^{-1} extending to $z = 8$ kpc, a value that is identical with the one found in this study for $z < 15$ kpc. Yoshii et al. (1987) derived a metallicity gradient of -0.5 ± 0.1 dex kpc^{-1} for $z \leq 2$ kpc in logarithmic scale from *UBV* star-count data by assuming the solar abundance in the Galactic plane, while this value is slightly steeper than the value of -0.37 dex kpc^{-1} for $z < 4$ kpc in this study. Jönch-Sörensen (1994) observed a sample of faint F dwarfs in order to investigate the spatial distribution of metallicity in the disk of the Galaxy. They found a vertical gradient of -0.33 dex kpc^{-1} for $z \leq 500$ pc and -0.19 dex kpc^{-1} for $500 \leq z \leq 1500$ pc. Trefzger et al. (1995) found a rather steep mean metallicity gradient of -0.55 ± 0.1 dex kpc^{-1} up to $z = 900$ pc and determined an overall gradient of -0.23 dex kpc^{-1} for $z < 4$ kpc; this gradient is slightly flatter than the one found in this study. We note that these results are in close agreement, both quantitatively and qualitatively, with our finding at the high-latitude fields. In § 6, our results are similarly interpreted as a mixture of stellar population with different mean metallicities at all z levels.

6. THE METALLICITY GRADIENT ARISING FROM THE POPULATION GRADIENT

A crucial aid to the interpretation of these metallicity gradients is the varying contributions from the different Galactic components. As shown in Figure 6, the expected relative number of stars from different components of the Galaxy is a function of height from the Galactic plane. The components are the thin disk, thick disk, and halo. The thin-disk population contains a young (age ≤ 3 Gyr), metal-rich population (mean abundance $\langle[\mathrm{Fe/H}]\rangle \sim 0.0$; $\sigma_{[\mathrm{Fe/H}]} \sim 0.15$), and a older (age ≥ 3 Gyr), more metal-poor population (mean abundance $\langle[\mathrm{Fe/H}]\rangle \sim -0.3$; $\sigma_{[\mathrm{Fe/H}]} \sim 0.2$) (Gilmore & Wyse 1985). The younger population contains ~20% of the stars near the Sun and has a vertical scale height or ~100 pc. The older population contains ~80% of the stars near the Sun and is characterized by a exponential scale height of ~300 pc. The young

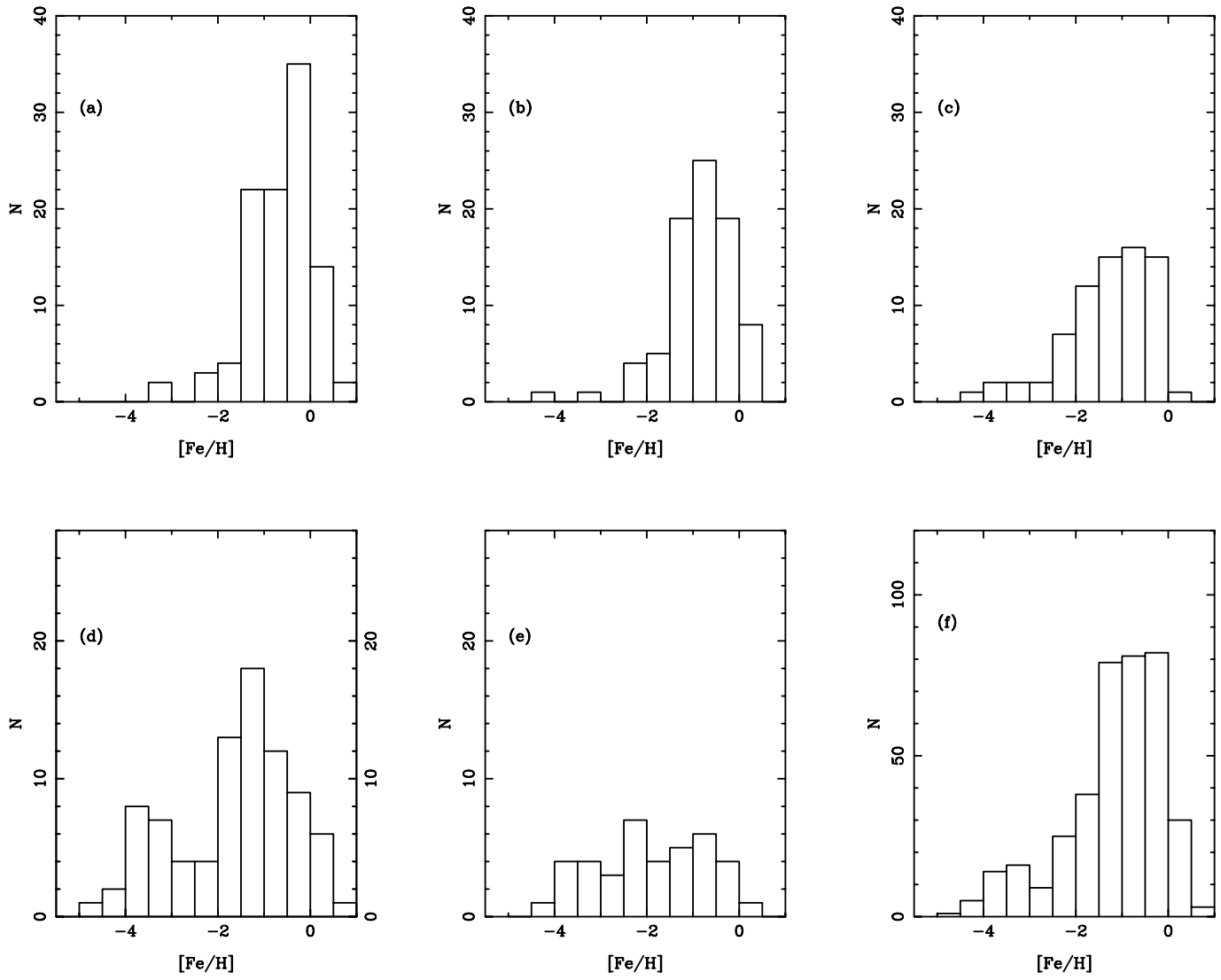

FIG. 7.—Metallicity distribution for sample stars as functions of apparent magnitude i. (a) $14.0 < i \leq 15.5$, (b) $15.5 < i \leq 16.5$, (c) $16.5 < i \leq 17.5$, (d) $17.5 < i \leq 18.5$, (e) $i > 18.5$, and (f) $14.0 < i \leq 20.5$.

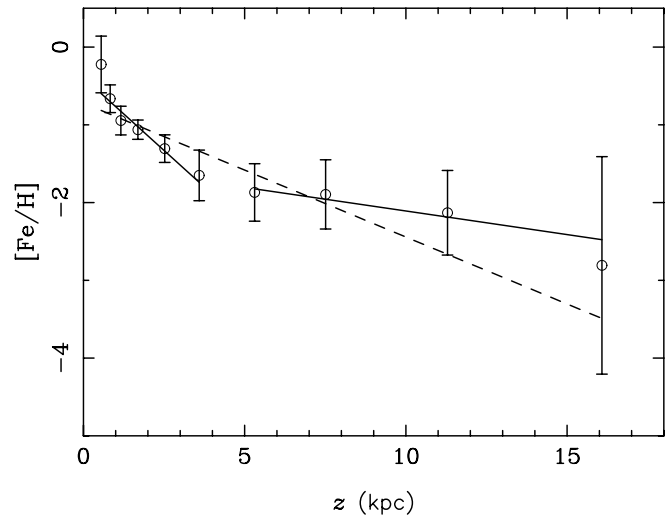

FIG. 8.—Mean metallicity distribution vs. mean z distance (in kiloparsecs) for 10 z intervals, showing a metallicity gradient $d[\mathrm{Fe/H}]/dz \sim -0.37$ dex kpc^{-1} for $z < 4$ kpc and $d[\mathrm{Fe/H}]/dz \sim -0.06$ dex kpc^{-1} (or possibly zero) between 5 and 15 kpc.

thin-disk stars contribute up to z heights of around 300 pc, and these old thin-disk stars dominate from 300 pc to 1 kpc. Here we consider only the old thin-disk population in our model, since we have very few samples of very nearby stars.

For the thick disk, Hartkopf & Yoss (1982) derived the mean abundance $\langle[\mathrm{Fe/H}]\rangle \sim -0.6$ and $\sigma_{[\mathrm{Fe/H}]} \sim 0.3$ with distances between 1 and 2 kpc; Buser et al. (1999) also derived the mean metallicity of the thick disk $\langle[\mathrm{Fe/H}]\rangle \sim -0.63$ and dispersion $\sigma_{[\mathrm{Fe/H}]} \sim 0.4$ dex. Chiba & Beers (2000) showed that the thick disk population includes stars with a wide range of metallicity, from $-2.2 \leq [\mathrm{Fe/H}] \leq -0.5$, and most of stars are in the richer end of this range. Recently, on the basis of medium-resolution spectroscopy and broadband photometry, Beers et al. (2002) found that the local fraction of metal-poor stars that might be associated with the metal-weak thick disk is on the order of 30%–40% at abundances below $[\mathrm{Fe/H}] = -1.0$. At the same time, they also found that this relatively high fraction of local metal-poor stars may extend to metallicities below $[\mathrm{Fe/H}] = -1.6$, much lower than what had been considered before. For the halo, the field stars have similar mean metallicity as globular clusters in the Milky Way. However, the halo field stars extend to much lower metallicity ($[\mathrm{Fe/H}] \simeq -5$) than do the globular

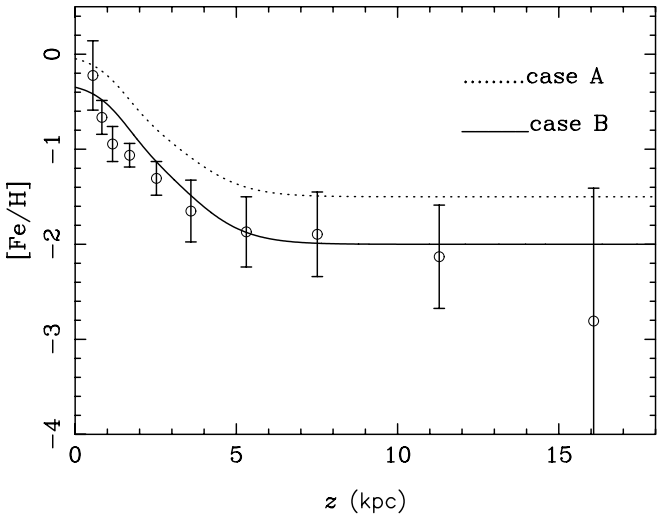

FIG. 9.—Observed and calculated mean metallicity distribution as a function of height z. The results of case A (*dotted line*) and case B (*solid line*) are illustrated.

clusters ($[\mathrm{Fe/H}] \simeq -2.2$) (Freeman & Bland-Hawthorn 2002). In general, the values adopted here are that the halo mean abundance $\langle[\mathrm{Fe/H}]\rangle \sim -1.5$ and $\sigma_{[\mathrm{Fe/H}]} \sim 0.5$ (Gilmore & Wyse 1985).

In this study, we try to estimate the metallicity gradient resulting from changing relative proportions of different populations, assuming there does not exist a gradient for a single population. The number of stars at different heights z for three components (Fig. 6) could be combined with mean metallicity to produce estimates of metallicity distributions as a function of height above the plane. To check the mean metallicity's effect on the gradient, we divide the mean metallicities into two cases for discussion. In case A, the mean metallicities are $\langle[\mathrm{Fe/H}]\rangle \sim 0.0$ for the thin disk, $\langle[\mathrm{Fe/H}]\rangle \sim -0.6$ for the thick disk, and $\langle[\mathrm{Fe/H}]\rangle \sim -1.5$ for the halo, respectively. In case B, the mean metallicities are $\langle[\mathrm{Fe/H}]\rangle \sim -0.3$ for the thin disk, $\langle[\mathrm{Fe/H}]\rangle \sim -1.0$ for the thick disk, and $\langle[\mathrm{Fe/H}]\rangle \sim -2.0$ for the halo, respectively. The mean parameter values in case A are in agreement with the majority of recent determinations, while the values in case B lie in the range of error of case A. The results are illustrated in Figure 9; the dotted line and solid line represent case A and case B, respectively. The open circles represent the observational data. Many factors affect the determination of mean metallicity. The first source contributing to errors is from photometric errors; the second from stellar metallicity by fitting SEDs. In addition, there may exist an error from the incompleteness of samples in each bin. As Figure 9 shows clearly, although case B matches the observed metallicity distribution, both cases exhibit similar gradients for $z < 5$ kpc, and they become flat for $z > 5$ kpc. Thus, the gradient we derived (-0.37 ± 0.1 dex kpc^{-1} for $z < 4$ kpc) can be interpreted as resulting from the different contributions in density distribution for the three components of the Galactic model, whereas the small or zero gradient $d[\mathrm{Fe/H}]/dz = -0.06 \pm 0.09$ cannot be interpreted as being caused by the different contributions from three components. In particular, the last data point ($z \sim 15$ kpc) can be attributed to the incompleteness of the sample at that large distance. So it is possible that there is a little or no gradient for $z > 5$ kpc. It should be noted that the low mean metallicity in case B is presumably a consequence of selection effects (such as magnitude, color selection, and distance selection) involved in the definition of the sample. But this is unimportant for the derivation of the gradient.

7. CONCLUSIONS AND SUMMARY

In this work, based on the BATC multicolor photometric system, we develop a calibration of temperature and metallicity for the dwarfs by employing a set of synthetic flux spectra calculated from theoretical models. Some temperature-sensitive color indexes in the BATC filter system are found to yield well-defined liner relations with $\log T_{\mathrm{eff}}$ (see Fig. 3). More importantly, this study shows that in using the BATC multicolor observations, we can not only conveniently assess stellar temperature but metallicity and gravity as well. We thus have confirmed the possibility of successfully classifying stars in three-dimensions from the BATC SEDs.

In addition, in this paper, by using F/G dwarfs of two BATC fields, we determined average stellar metallicity as a function of distance from the Galactic plane. It can clearly be seen that mean metallicity decreases with increasing z; that is, we find a gradient of -0.37 ± 0.1 dex kpc^{-1} for $z < 4$ kpc, whereas the data show a weak gradient between 5 and 15 kpc, i.e., $d[\mathrm{Fe/H}]/dz = -0.06 \pm 0.09$ dex kpc^{-1}. The overall distribution shows a metallicity gradient $d[\mathrm{Fe/H}]/dz = -0.17 \pm 0.04$ dex kpc^{-1}, up to 15 kpc. These results are in agreement with the values in the literature (Yoshii et al. 1987; Yoss et al. 1987; Trefzger et al. 1995). In our study, these results are interpreted as different contributions from three components of the Galaxy at different z distances. In star counts the younger metal-rich stars are confined to regions close to the Galactic mid-plane, while the older, metal-poorer stars with a larger scale height dominate at larger vertical distances from the Galactic plane. As a consequence, a vertical metallicity gradient is caused by the varying dominance of different stellar components of the Galaxy. It is possible that additional observational investigations will give more evidence for the metallicity gradient of the Galaxy and therefore provide a powerful clue to the disk and halo formation, because it almost certainly concerns events during and shortly after the early Galactic collapse and the beginning of disk formation (Sandage 1981; Bell 1996; Norris & Ryan 1991).

We would like to thank the referee, K. Yoss, for his insightful comments and suggestions, which improved this paper greatly. The BATC Survey is supported by the Chinese Academy of Sciences, the Chinese National Natural Science Foundation under the contract No. 10273012, and the Chinese State Committee of Sciences and Technology. This work has been supported by the National Key Basic Research Science Foundation (NKBRSF TG199075402). We also thank the assistants who helped with the observations for their hard work and kind cooperation.

REFERENCES

Ardeberg, A., Lindgren, H., & Nissen, P. E. 1983, A&A, 128, 194
Beers, T. C., Flynn, K., & Gebhardt, K. 1990, AJ, 100, 32
Beers, T. C., et al. 2002, AJ, 124, 931
Bell, D. J. 1996, PASP, 108, 1139
Buser, R., & Rong, J. X. 1995, in IAU Symp. 169, Unresolved Problems of the Milky Way, ed. L. Biltz (Dordrecht: Kluwer), 427
Buser, R., Rong, J. X., & Karaali, S. 1999, A&A, 348, 98
Cameron, L. M. 1985, A&A, 147, 47

Carraro, G., Ng, Y. K., & Portinari, L. 1998, MNRAS, 296, 1045
Chen, A. B., Tsay, W., Tsai, W., & Lu, P. K. 2000a, AJ, 120, 2569
Chen, B., Stoughton, C., & Smith, J. A. 2001, ApJ, 553, 184
Chen, L., Hou, J. L., & Wang, J. J. 2003, AJ, 125, 1397
Chen, Y. Q., Nissen, P. E., Zhao, G., Zhang, H. W., & Benoni, T. 2000b, A&AS, 141, 491
Chiba, M., & Beers T. 2000, AJ, 119, 2843
Crawford, D. L. 1975a, AJ, 80, 955
Du, C. H., et al. 2003, A&A, 407, 541
Fan, X. H., et al. 1996, AJ, 112, 628
Fenkart, R., & Esin-Yilmaz, F. 1985, A&AS, 62, 39
Freeman, K., & Bland-Hawthorn, J. 2002, ARA&A, 40, 487
Friel, E. D. 1988, AJ, 95, 1727
———. 1995, ARA&A, 33, 381
Gilmore, G., & Reid, N. 1983, MNRAS, 202, 1025
Gilmore, G., & Wyse, R. F. G. 1985, AJ, 90, 2015
Gilmore, G., Wyse, R. F. G., & Kuijken, K. 1989, ARA&A, 27, 555
Grenon, M. 1977, in Highlights Astron., 4, 55
Hartkopf, W. I., & Yoss, K. M. 1982, AJ, 87, 1679
Henry, R. B. C., & Worthey, G. 1999, PASP, 111, 919
Hou, J. L., Prantzos, N., & Boissier, S. 2000, A&A, 362, 921
Jenkner, H., et al. 1990, AJ, 99, 2082
Jönch-Sörensen, H. 1994, Ph.D. thesis, Copenhagen Univ.
Karaali, S., Ak, S. G., & Bilir, S., Karatas, Y., & Gilmore, G. 2003, MNRAS, 343, 1013
Kroupa, P., Tout, C. A., & Gilmore, G. 1993, MNRAS, 262, 545
Lejeune, T., Cuisinier, F., & Buser, R. 1997, A&AS, 125, 229
Maciel, W. J., Costa, R. D. D., & Uchida, M. M. M. 2003, A&A, 397, 667
Majewski, S. R. 1992, ApJS, 78, 87
Majewski, S. R. 1993, ARA&A, 31, 575
Neese, C. L., & Yoss, K. M. 1988, AJ, 95, 463
Nissen, P. E. 1981, A&A, 97, 145
Norris, J., & Green, E. M. 1989, ApJ, 337, 272
Norris, J., & Ryan, S. G. 1991, ApJ, 380, 403
Ojha, D. K., Bienaymé, O., Robin, A. C., & Crézé, M. 1996, A&A, 311, 456
Oke, J. B., & Gunn, J. E. 1983, ApJ, 266, 713
Olsen, E. H. 1988, A&A, 189, 173
Pasquali, A., & Perinotto, M. 1993, A&A, 280, 581
Piatti, A. E., Claria, J. J., & Abadi, M. G. 1995, AJ, 110, 2813
Pickles, A. J. 1998, PASP, 110, 863
Ratnatunga, K. U., & Freeman, K. C. 1989, ApJ, 339, 126
Reid, N. I., & Majewski, S. R. 1993, ApJ, 409, 635
Robin, A. C., Haywood, M., & Crézé, M. 1996, A&A, 305, 125
Sandage, A. 1981, AJ, 86, 1643
———. 1990, JRASC, 84, 70
Sandage, A., & Fouts, G. 1987, AJ, 93, 74
Schuster, W. J., & Nissen, P. E. 1989, A&A, 221, 65
Shaver, P. A., et al. 1983, MNRAS, 204, 53
Stetson, P. B. 1987, PASP, 99, 191
Trefzger, C. H., Pel, J. W., & Gabi, S. 1995, A&A, 304, 381
Wallerstein, G. 1962, ApJS, 6, 407
Xia, L. F., et al. 2002, PASP, 114, 1349
Yamagata T., & Yoshii, Y. 1992, AJ, 103, 117
Yoshii, Y., Ishida, K., & Stobie, R. S. 1987, AJ, 93, 323
Yoss, K. M., & Hartkopf, W. I. 1979, AJ, 84, 1293
Yoss, K. M., Neese, C. L., & Hartkopf, W. I. 1987, AJ, 94, 1600
Zhou, X., et al. 2001, Chinese J. Astron. Astrophys., 1, 372
———. 2003, A&A, 397, 361